AIP Journal of Applied Physics

Sharp reduction of the secondary electron emission yield from grooved surfaces

M. Pivi, F. K. King, R. E. Kirby, T. O. Raubenheimer, G. Stupakov, and F. Le Pimpec

Citation: Journal of Applied Physics **104**, 104904 (2008); doi: 10.1063/1.3021149
View online: http://dx.doi.org/10.1063/1.3021149
View Table of Contents: http://scitation.aip.org/content/aip/journal/jap/104/10?ver=pdfcov
Published by the AIP Publishing

Articles you may be interested in

Secondary electron yield on cryogenic surfaces as a function of physisorbed gases
J. Vac. Sci. Technol. A **30**, 051401 (2012); 10.1116/1.4736552

Contribution of surface plasmon decay to secondary electron emission from an Al surface
Appl. Phys. Lett. **99**, 184102 (2011); 10.1063/1.3658455

Electron inelastic scattering and secondary electron emission calculated without the single pole approximation
J. Appl. Phys. **104**, 114907 (2008); 10.1063/1.3033564

Influence of electron irradiation and heating on secondary electron yields from non-evaporable getter films observed with in situ x-ray photoelectron spectroscopy
J. Vac. Sci. Technol. A **25**, 675 (2007); 10.1116/1.2738491

X-ray photoelectron spectroscopy and secondary electron yield analysis of Al and Cu samples exposed to an accelerator environment
J. Vac. Sci. Technol. A **21**, 1625 (2003); 10.1116/1.1593051

SHIMADZU
Excellence in Science
Powerful, Multi-functional UV-Vis-NIR and FTIR Spectrophotometers
Providing the utmost in sensitivity, accuracy and resolution for applications in materials characterization and nano research
• Photovoltaics • Ceramics
• Polymers • DNA film structures
• Thin films • Coatings
• Paints • Packaging materials
Click here to learn more

[This article is copyrighted as indicated in the article. Reuse of AIP content is subject to the terms at: http://scitation.aip.org/termsconditions. Downloaded to] IP: 35.8.11.3 On: Mon, 25 Jan 2016 00:27:02

Sharp reduction of the secondary electron emission yield from grooved surfaces

M. Pivi,[1,a)] F. K. King,[1] R. E. Kirby,[1] T. O. Raubenheimer,[1] G. Stupakov,[1] and F. Le Pimpec[2]
[1]*Stanford Linear Accelerator Center, Menlo Park, California 94025, USA*
[2]*Paul Scherrer Institute, 5232 Villigen, Switzerland*

(Received 28 November 2007; accepted 4 October 2008; published online 18 November 2008)

The effect of an artificially enhanced rough surface on the secondary electron yield (SEY) was investigated both theoretically and experimentally. Analytical studies on triangular and rectangular grooved surfaces show the connection between the characteristic parameters of a given geometry to the SEY reduction. The effect of a strong magnetic field is also discussed. SEY of grooved samples have been measured and the results agree with particle simulations using a Monte Carlo approach.
© *2008 American Institute of Physics*. [DOI: 10.1063/1.3021149]

I. INTRODUCTION

In the quest of suppressing multipactor discharge and electron cloud effects (ECEs) for future colliders, several methods are under study to lower the secondary electron yield (SEY). The SEY represents the number of emitted secondary electrons per primary incident electron and is also known in the literature as secondary emission yield. Historically, much of the work done to suppress multipacting was developed in the klystron industry.[1–3] However, the methods used today are in many cases still based on that early work.[4] These include special coatings on metal or ceramic surfaces, surface cleaning, beam conditioning, and the use of rough or porous surfaces.[5–8] For the positron damping ring (DR) of the International Linear Collider (ILC), it is mandatory for the SEY to be below 1.2 in order to avoid ECE.[9,10] This specification for the SEY refers to magnetic field regions, where the electron cloud buildup is expected to be severe. It is also important to realize that the beam itself and the ECE associated with it will condition the surface. However, it is imperative to use low SEY materials as a starting point, in order to reduce the *in situ* commissioning time. In this paper, we will look, theoretically and experimentally, at the effect and effectiveness of artificially grooving metal surfaces on the SEY.

Based on prediction of reduction in the SEY due to artificially enhanced surface roughness with triangular grooves,[11] an experimental program was started at Stanford Linear Accelerator Center (SLAC) for triangular and rectangular grooves.[12] In this paper we consider two types of grooves, triangular grooves with angle α and rectangular characterized by the period b, dwell width a, depth h, and a flat top thickness t. Furthermore, we have also considered a rectangular groove samples with inclined (slanted) walls with respect to the surface normal, thus combining aspects of the rectangular groove and the inclined walls of the triangular groove. An initial electron whose trajectory, in Fig. 1, is shown in red hits the surface at point A and produces secondary electrons shown with blue lines. Depending on the emission angle, some of the secondary electrons can escape the groove and move away from the surface. Other secondary electrons would hit an inner side of the groove. With some probability they will be absorbed, or they can generate further secondary electrons (which are *second generation* secondaries) whose trajectories are shown in green. The process may repeat several times until the energy of higher generations becomes too low and they are absorbed by the surface.

Note that although collisions of secondaries with side walls of the grooves would lead to suppression of the SEY, there is a competing mechanism for triangular grooves that increases the yield. It is due to the fact that a primary electron that is incident perpendicular to the horizontal plane in Fig. 1(a) hits the groove surface at an angle $(\pi-\alpha)/2$ relative to the sample normal. Since the SEY typically increases toward grazing angle, the number of secondaries will be larger than for a normal incidence on a flat surface. Thus, it is not obvious whether triangular grooves suppress the effective emission or increase it for a given angle α. Simulation

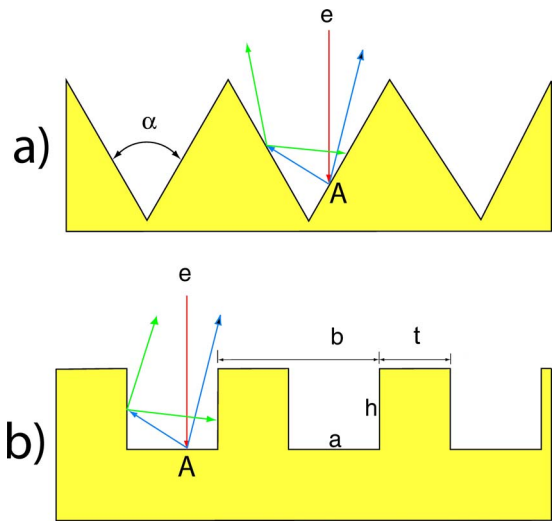

FIG. 1. (Color online) (a) Triangular and (b) rectangular grooves on the surface. Triangular grooves are characterized by the angle α. Rectangular grooves have a period b, dwell width a, depth h, and a flat top thickness t.

a)Electronic address: mpivi@slac.stanford.edu.

 © 2008 American Institute of Physics

[This article is copyrighted as indicated in the article. Reuse of AIP content is subject to the terms at: http://scitation.aip.org/termsconditions. Downloaded to] IP: 35.8.11.3 On: Mon, 25 Jan 2016 00:27:02

results might depend on the specific model of secondary emission. In general, simulations show that a smaller angle results in a lower SEY. Rounding of the tips of the triangular grooves (which is likely to occur in a manufacturing extrusion process for example) generally reduces the performance of the grooves since it reduces the electron trapping probability given by the inclined surface.

In our simulation code, we used a subroutine from the POSINST computer code[13] to calculate probability of emission, with a given energy and angular coordinates of the secondary electron. The model implemented in this subroutine is described in Ref. 14. The angular distribution of secondaries is assumed $\propto \cos\theta$, where θ is the angle with the normal to the surface, and the incidence-angle dependence of the SEY δ is given by the relation $\delta \propto [1+r_1(1-\cos^{r_2}\theta)]$, where r_1 and r_2 are positive numbers that depend on the properties of the surface. In the simulation we assumed that primary electrons hit the surface normal to the averaged plane (as shown in Fig. 1). To make calculations faster, we simulated only first two or three generations of the electrons with about 2×10^4 incident electrons per groove. An effective SEY was obtained by averaging over the groove period. The secondary energy spectrum is a fundamental parameter used in the simulation to take into account the energy distribution of the emitted electrons at the location of the primary incident electron. The emitted energy spectrum of the secondary electrons $d\delta/dE$ can be computed as

$$\frac{d\delta}{dE} = f_{1,e} + f_{1,r} + \frac{d\delta_{ts}}{dE}, \tag{1}$$

where

$$\frac{d\delta_{ts}}{dE} = \sum_{n=1}^{\infty} \frac{nP_{n,ts}(E_0)(E/\epsilon_n)^{p_n-1}e^{-E/\epsilon_n}}{\epsilon_n \Gamma(p_n) P(np_n, E_0/\epsilon_n)} \times P[(n-1)p_n, (E_0-E)/\epsilon_n] \tag{2}$$

represents the energy distribution of the so-called true secondary electrons to be distinguished from the energy distribution $f_{1,e}$ of the elastically reflected electrons and the energy distribution $f_{1,r}$ of the rediffused electrons from the bulk of the material.[14] The index ts is for true secondary, $P_{n,ts}$ is the probability for emitting n true-secondary electrons, E_0 and E are the primary and secondary electron energies, ϵ_n and p_n are phenomenological fitting parameters, $P(z,x)$ the incomplete gamma function, and $\Gamma(x)$ is the gamma function.

The conventional picture of secondary emission can be summarized as follows: when a steady current of electrons impinges on a surface, a certain portion I_e is backscattered elastically while the rest penetrates into the material. Some of these electrons inelastically scatter from one or more atoms inside the material and are reflected back out. These are the so-called "rediffused" electrons, and we call the corresponding current I_r. The rest of the electrons interact in a more complicated way with the material and yield the so-called "true-secondary electrons," whose current we call I_{ts}. The yields for each type of electron are combined linearly to give the total SEY of the material.

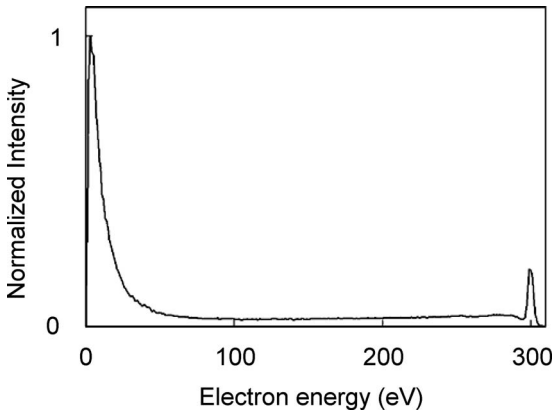

FIG. 2. Measured energy distribution of secondary electrons emitted by an unconditioned stainless steel sample when impacted by a 300 eV incident electron beam. Data courtesy of R. Kirby.

The energy distribution of the secondary electrons emitted from an unconditioned stainless steel surface by a 300 eV incident primary electron beam is shown in Fig. 2, most of the secondaries having an energy comprised between 0 and 50 eV. We define that to be the true secondary electrons. The peak of elastically reflected electrons is visible at 300 eV, while the 50 and 300 eV ranges are composed of inelastically rediffused electrons. At 3 keV primary electron energy, the energy distribution of the secondaries is very similar with a decreased elastic peak and a longer inelastic component.

II. GROOVED SURFACES SIMULATION RESULTS

It is interesting to note that the effective SEY does not depend on the size of the triangular grooves and is only a function of the angle α. This gives certain flexibility in the practical choice of the dimensions of the grooves. This independence of SEY on the size of the grooves breaks down when the size of the groove becomes comparable to the penetration depth of the incident electrons in metal.

The result of simulations for triangular grooves with angle $\alpha=60°$ on a copper surface with maximum SEY $\delta_{\max}=1.75$ is shown in Fig. 3. The top curve gives the reference value of $\delta(E)$ (where E is the incident energy of the primary electron) for a flat surface (without grooves) at normal inci-

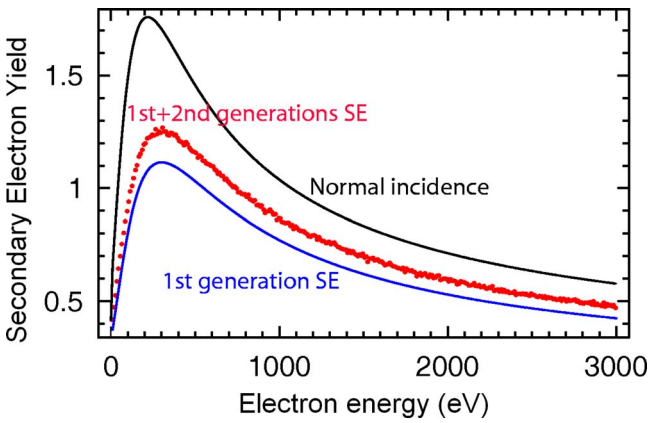

FIG. 3. (Color online) SEY as a function of incident energy for triangular grooves with $\alpha=60°$.

[This article is copyrighted as indicated in the article. Reuse of AIP content is subject to the terms at: http://scitation.aip.org/termsconditions. Downloaded to] IP: 35.8.11.3 On: Mon, 25 Jan 2016 00:27:02

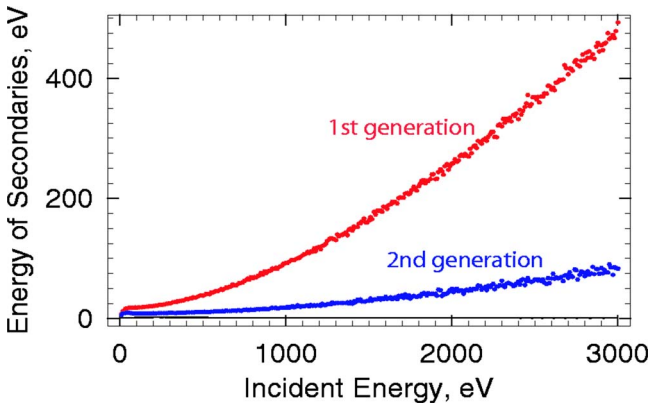

FIG. 4. (Color online) Energy of secondary electrons for triangular grooves with $\alpha=60°$.

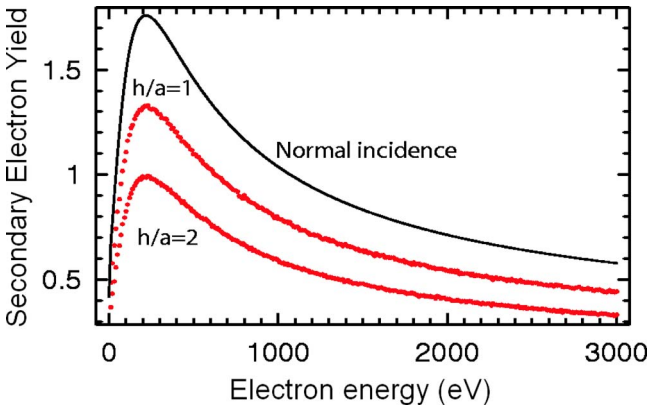

FIG. 6. (Color online) Rectangular grooves with $a=\frac{2}{3}b$.

dence. The blue curve is the effective SEY with grooves when only first generation of secondaries is taken into account (that is, each secondary electron is assumed to disappear when it hits a wall). The red dots show the result of simulation with two generations of secondaries taken into account (second generation secondary electrons do not produce secondaries when they hit the wall). As is seen in the picture, the maximum effective SEY decreases to a value of about 1.3 in this case.

The average energy computed from the secondary electron energy distribution of first and second generations as a function of the primary electron energy is shown in Fig. 4. With each consecutive generation of secondaries, the average energy decreases and for the second generation, it becomes smaller than the energy corresponding to the maximum of SEY (about 200 eV). This decrease in the average energy for higher generations of secondary electrons indicates that they should not contribute much to the total effective yield for a grooved surface.

In Fig. 5, we compare results for grooves with the angle α equal to 40° and 60° (and the reference case of the flat surface for normal incidence). As expected, the smaller angle results in the stronger suppression of the emission, with the maximum value of δ for $\alpha=40°$ approximately equal to $\delta_{max}=0.9$.

Figure 6 shows results of the simulation for rectangular grooves with $a=\frac{2}{3}b$. Two red dotted lines correspond to different aspect ratios of the grooves: the bottom one is for $h/a=2$ and the middle one corresponds to $h/a=1$. The top curve gives the reference value of $\delta(E)$ for a flat surface for normal incidence. Deeper rectangular grooves show larger suppression of secondary emission.

We also simulate the variation in the SEY with the rectangular groove parameters. Figure 7 shows the dependence of the yield with the period-to-depth ratio h/b and for different width-to-thickness a/t values. For these simulations, we have assumed a reference flat surface without grooves with a peak SEY of 1.75.

We manufactured a rectangular-grooved sample in copper oxygen-free electronic material and measured the SEY in the analysis chamber. Sample dimensions are $h=5$, $b=2$, $a=1.8$, and $t=0.25$ mm, and thus with a ratio $a/t=7.2$. On the lower right of Fig. 7, the expected SEY from simulations for a sample with the above dimensions is compared to the measurements. Both measurements and simulations confirm that the SEY is well below one. The difference between measurements and simulations is within an error of 10%–15%. Figure 7 shows that a good reduction in the SEY for rectangular

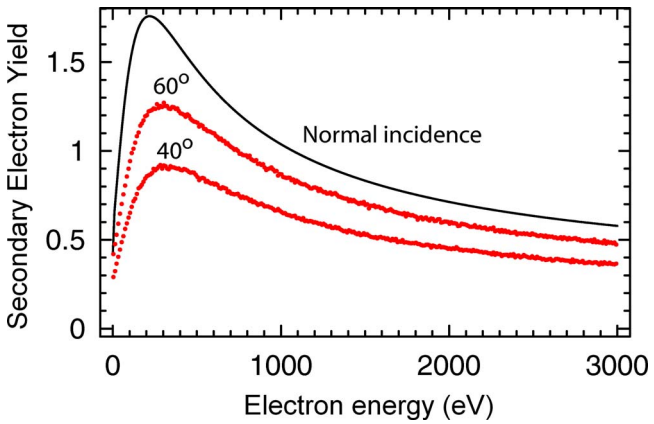

FIG. 5. (Color online) Comparison of the effective SEY for 60° and 40° grooves.

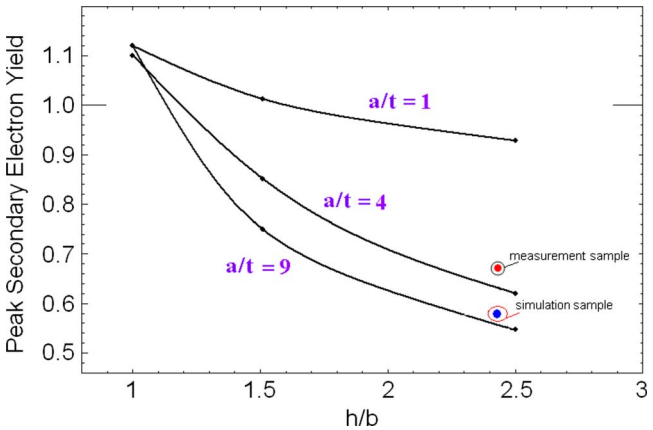

FIG. 7. (Color online) Simulation of SEY, of rectangular grooves in magnetic field free region, as a function of h/b ratio for different a/t ratios, where t is the thickness of the flat top groove. On the lower right is also shown the expected SEY of a copper sample compared to effective measurements, with sample dimensions $h=5$, $b=2$, $a=1.8$, and $t=0.25$ mm and thus $a/t=7.2$. For the simulation, the reference flat top surface has a peak SEY of 1.75.

[This article is copyrighted as indicated in the article. Reuse of AIP content is subject to the terms at: http://scitation.aip.org/termsconditions. Downloaded to] IP: 35.8.11.3 On: Mon, 25 Jan 2016 00:27:02

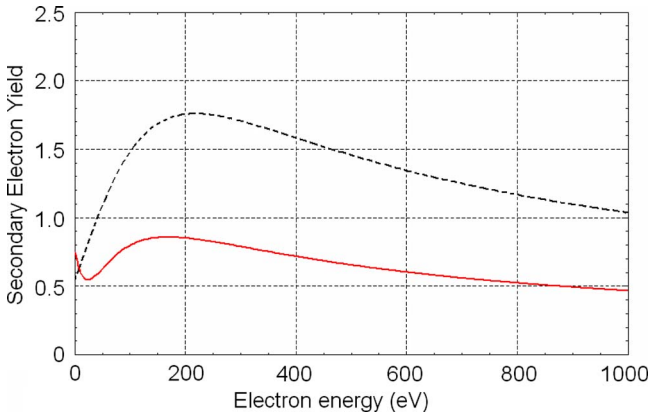

FIG. 8. (Color online) Simulation of SEY of rectangular grooves in 0.2 T magnetic field. The SEY of a flat surface used as reference in field free region is shown in dashed line. Solid line represents rectangular groove surface with parameters: period=0.25, depth=0.25 and width=0.025 mm.

grooves is obtained with a large depth-to-period ratio h/b and a large dwell width-to-thickness ratio a/t.

III. EFFECT OF MAGNETIC FIELD

Even a weak magnetic field will change the orbits of secondary electrons and affects their collisions with grooved surfaces. In particle accelerators, the typical magnetic field value is 0.1–1 T, which results in small electron radius of gyration. For example, the Larmor radius r_L of a 200 eV electron in a 1 T magnetic field is about 47 μm, small compared to the groove size. In the limit of the gyration radius r_L being much smaller than the size of the triangular grooves, the effective SEY is a function only of the angle α and does not depend on r_L nor on the height of the grooves. In fact, in the limit $r_L \to 0$, most of the just-born secondary electrons in their initial spiraling motion collide with the tilted groove surface in the immediate vicinity of their emission point. The smaller the angle α, the larger will be the collision probability of the secondary electrons with the wall.

In a dipole field, rectangular grooves are efficient if the dwell width a is comparable with the electron Larmor diameter or $a \sim 2r_L$. In this limit, the electrons most likely collide with the groove wall and the secondary electrons are likely to hit the same side of the wall in their spiraling motion. The groove efficiency reduces if $a \gg 2r_L$, since most likely incoming electrons spiral inside the space between the groove walls. They generate secondary electrons at the base of the groove and the secondary electrons spiral out without hitting the walls. Small thickness t and large depth h also increase the efficiency of rectangular grooves in a dipole field.

We have simulated two different cases of grooves in a 0.2 T magnetic field. The field applied in the simulation is perpendicular to the substrate of the groove sample. The Larmor radius in such magnetic field is about 240 μm for a 200 eV electron. This is the typical magnetic field of ILC positron DR dipoles. The simulation results for a rectangular groove sample with $b=250$ μm are shown in Fig. 8; the peak secondary yield can be lowered below 1.

The figure shows that the SEY at a very low primary electron energy increased as the energy decreased. In the presence of a dipole field, we speculate that electrons at very low energies are likely to enter the groove area without hitting the side walls, since their Larmor radius is small and $a \gg 2r_L$. They generate secondary electrons at the base of the groove and the secondary electrons spiral out without hitting the walls. Furthermore, the primary electrons hit the base of the groove with a grazing angle due to their spiraling motion. As mentioned in Sec. I, the SEY typically increases with grazing angles. This may well explain the SEY increase at very low energy in Fig. 8.

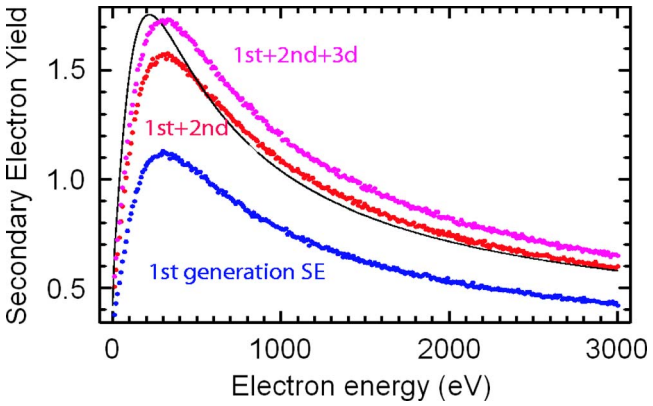

FIG. 9. (Color online) SEY in a 0.2 T magnetic field $\alpha=60°$.

The results for triangular grooves of angles $\alpha=60°$ and $\alpha=40°$ are shown in Figs. 9 and 10, respectively. The solid black curve in the plot is the reference curve of a flat surface with a $\delta_{max}=1.75$. Three color dotted curves show the effective SEY with one, two, or three generations of secondaries taken into account. Surprisingly, we found that with magnetic field, the contribution of higher generations of secondaries becomes more important than for the case without magnetic field. Our result shows that for 60° grooves, with three generation of secondaries, the total SEY actually exceeds the emission of a flat surface for energies above ≈300 eV. However, a smaller angle, 40°, shows a noticeable suppression in the energy range below 700 eV.

Simulations show that the trend of SEY reduction continues for smaller angles. A triangular groove angle of 20° is effective to decrease the SEY well below unity. For a more complete analysis of a triangular groove with smaller angles, see Refs. 15 and 16.

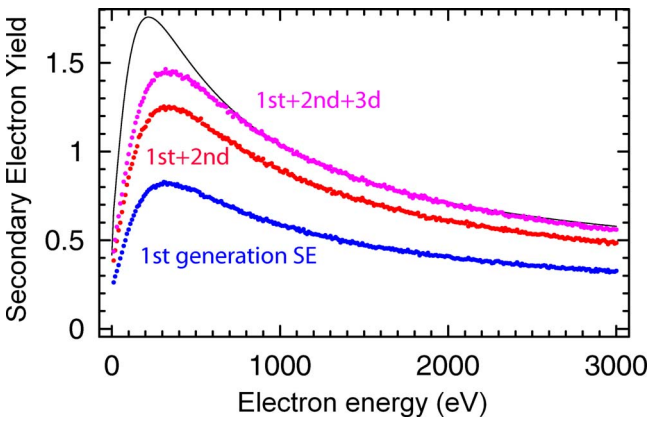

FIG. 10. (Color online) SEY in a 0.2 T magnetic field $\alpha=40°$.

[This article is copyrighted as indicated in the article. Reuse of AIP content is subject to the terms at: http://scitation.aip.org/termsconditions. Downloaded to] IP: 35.8.11.3 On: Mon, 25 Jan 2016 00:27:02

TABLE I. List of samples and test that were carried out on each.

Sample and No.	Side	Characteristics	Peak SEY	Figure
Al 6	Flat	···	3.25	11
Al 6	Triangular	$\alpha=40°$, $h=1$ mm	2.35	11
TiN/Al 6	Flat	···	1.7	11
TiN/Al 6	Triangular	$\alpha=40°$, $h=1$ mm	1.25	11
Al 7	Flat	···	3.3	12
Al 7	Triangular	$\alpha=40°$, $h=0.2$ mm	2.4	12
Cu 6	Flat	···	1.65	14
Cu 6 slanted	Rectangular	$h=1$ mm, $a=350$ μm, $t=50$ μm	0.85	14
Cu 7	Rectangular	$h=5$ mm, $a=1.8$ mm, $t=254$ μm	0.65	14 and 15
TiN/Al 10	Flat	···	1.5	18
TiN/Al 9 and 10	Rectangular	$h=5$ mm, $a=1.88$ mm, $t=600$ μm	0.75	18
TiZrV 7 nonactivated	Flat	···	1.8	Text, p. 7
TiZrV 7 activated[a]	Flat	···	1.2	Text, p. 7
TiZrV 8 nonactivated	Rectangular	$h=5$ mm, $a=1$ mm, $t=1$ mm	0.92	19
TiZrV 8 activated	Rectangular	$h=5$ mm, $a=1$ mm, $t=1$ mm	0.68	19

[a]Surface activation process consists on heating the sample for at least 200 °C, 2 h.

The use of sawtooth has been investigated to minimize the photodesorption outgassing of the chamber wall.[17] This idea was reused, in the case of the large hadron collider, to diminish the production of photoelectron from the copper beam screen, those photoelectrons being the main cause of the ECE.[18,19] A sawtooth design is also a possible remedy for the ECE in the ILC DR, where magnetic fields are present. More feasibility studies are needed before sawtooth could be considered in DR design, including an estimation of their efficiency and impedance.

IV. EXPERIMENTAL STUDIES

A. Experimental setup

The system used to measure the SEY is described in detail in (Ref. 20). Measuring techniques included x-ray photoelectron spectroscopy and residual gas analysis.

The SEY (δ) definition is determined from the following equations:

$$\delta = \frac{\text{number of electrons leaving the surface}}{\text{number of incident electrons}}, \tag{3}$$

$$\delta = 1 - \frac{I_T}{I_P}. \tag{4}$$

In practice Eq. (4) is used because it contains parameters directly measured in the retarding target potential experiment. I_P is the primary current (the current leaving the electron gun and impinging on the surface of the sample) and I_T is the total current measured on the sample ($I_T=I_P-I_{SE}$). I_{SE} is the secondary electron current leaving the target.

The SEY is measured, at normal incidence, by using a gun capable of delivering a scanning electron beam of 0–3 keV, working at a set current of 2 nA and having a 0.4 mm^2 spot size on the target. To scan grooved surfaces the gun can be set into a raster mode. In this mode the primary electron beam is rapidly deflected, like in a cathodic tube, and scans an area of a cm^2. For each given energy an average current over 100 measurements is returned to the computer by the electrometer. The variation between SEY measured on a flat surface in the raster mode versus the point mode is less than 2%, measurement obtained on a fully flat reference sample.

The measurement of the SEY is done while biasing the sample to −20 V. This retarding field repels most secondaries from adjacent parts of the system that are excited by the elastically reflected primary beam. The primary beam current as a function of the primary beam energy is measured and recorded each time before a SEY measurement, by biasing the target to +150 V, and with the same step in energy for the electron beam. A fresh current lookup table is created with each measurement. The SEY measurement, over the 0–3 keV range, takes around 5 min. The first point of the data is taken at 10 eV. At 0 eV, hence no primary electron beam, the SEY is artificially set to 1.

B. Experimental results

In order to obtain a variety of triangular groove profiles, the samples were machined by electrical discharge (EDM). All samples have a diameter of 2.54 cm. EDM creates a thick oxide of Al_2O_3 on the Al 6063 alloy, explaining the high value of the SEY maximum for the flat surface. All the SEY measurements presented in this paper were made in a magnetic-free region. All the groove measurements were obtained in a raster mode. Measurement on the flat part of a half grooved half flat sample was obtained on point mode.

A list of samples and test that were carried out on each sample is summarized in Table I.

The first experimental confirmation of the sharp reduction predicted by the simulation was obtained on triangular grooved sample made of Al 6063, and then coated with 130 nm of TiN, shown in Fig. 11. Another example of SEY reduction from a grooved Al sample is shown in Fig. 12. The grooves of this sample are 0.2 mm height with the angle $\alpha \sim 40°$. A similar reduction in the SEY is seen.

Recently some studies[15,16] have emphasized the important issue of the systematic effects introduced by nonideal features on grooved surfaces. In particular, the effect that rounding of the tips of triangular grooves (which is likely to

[This article is copyrighted as indicated in the article. Reuse of AIP content is subject to the terms at: http://scitation.aip.org/termsconditions. Downloaded to] IP: 35.8.11.3 On: Mon, 25 Jan 2016 00:27:02

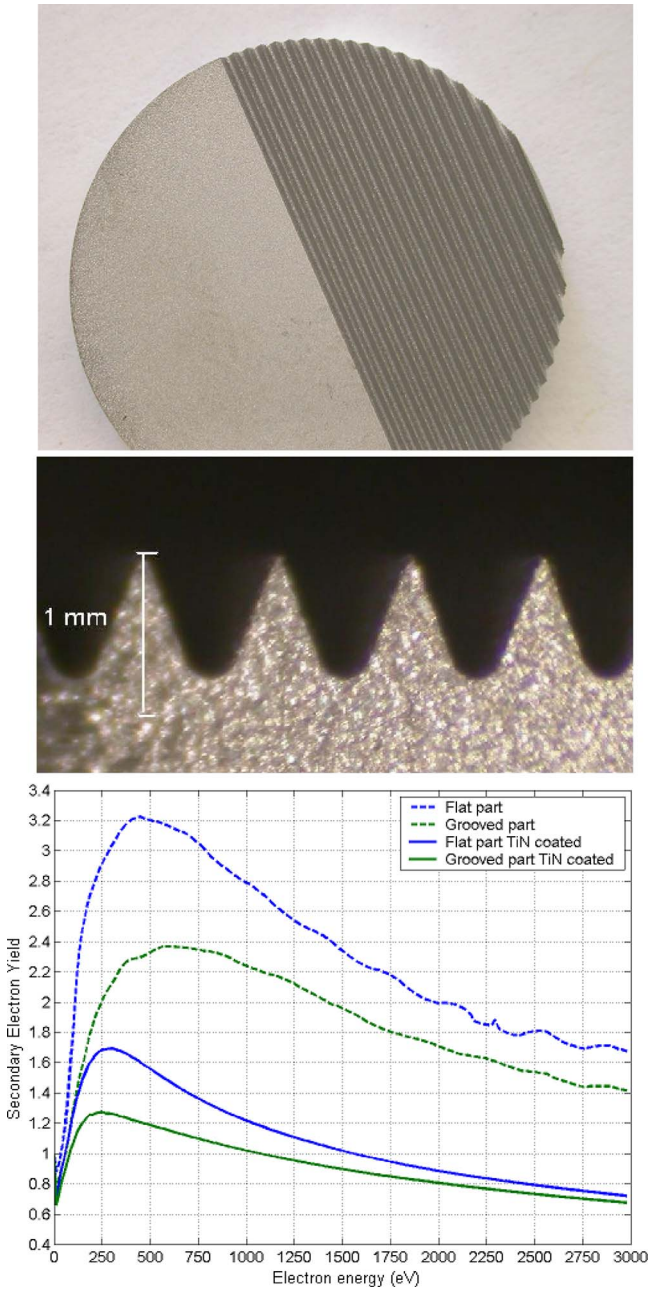

FIG. 11. (Color online) Al 6063 alloy sample half flat and half grooved, 1 inch diameter. Triangular grooves are 1 mm deep and full opening angle α is 40° (top). SEY results obtained, at normal primary incidence, before and after TiN coating (bottom).

occur in an extrusion process for example) has on the SEY performance. Typically, larger rounding results in a larger SEY.

Rectangular-grooved surfaces have been manufactured and tested. Figure 13 shows copper samples made with different geometries including a sample manufactured with slanted walls. The fully grooved rectangular sample has grooves of height $h=5$ mm, a distance between the right and left side of the grooves wall of $a=1.8$ mm, and a fin thickness of $t=0.254$ mm. The slanted wall of the second sample is inclined with a 20° angle and grooves dimensions are $h=1.0$, $a=0.35$, and $t=0.05$ mm.

Measurements of the SEY are shown in Figs. 14 and 15. In Fig. 14, the SEY of the slanted grooved sample is almost

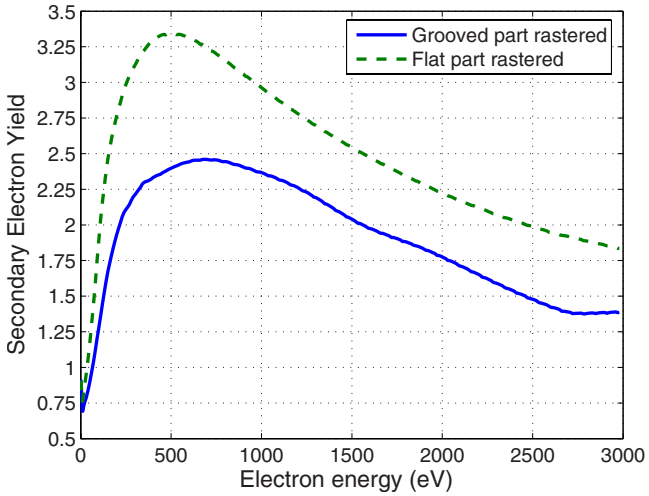

FIG. 12. (Color online) EDM Al sample 7 triangular grooves of $\alpha \sim 40°$ and a depth=0.2 mm.

50% (solid lines) reduced from the flat side. The effect of the rectangular grooves brings the reduction to 60% (dashed line). Simulation shows that for a ratio $h/a=2$ the reduction is close to 40%, Fig. 6. The h/a ratio for our sample is ~2.8, hence bringing more reduction, as expected from simulations.

We have investigated the effect of sample rotation relative to the surface normal and the angle of incidence of the

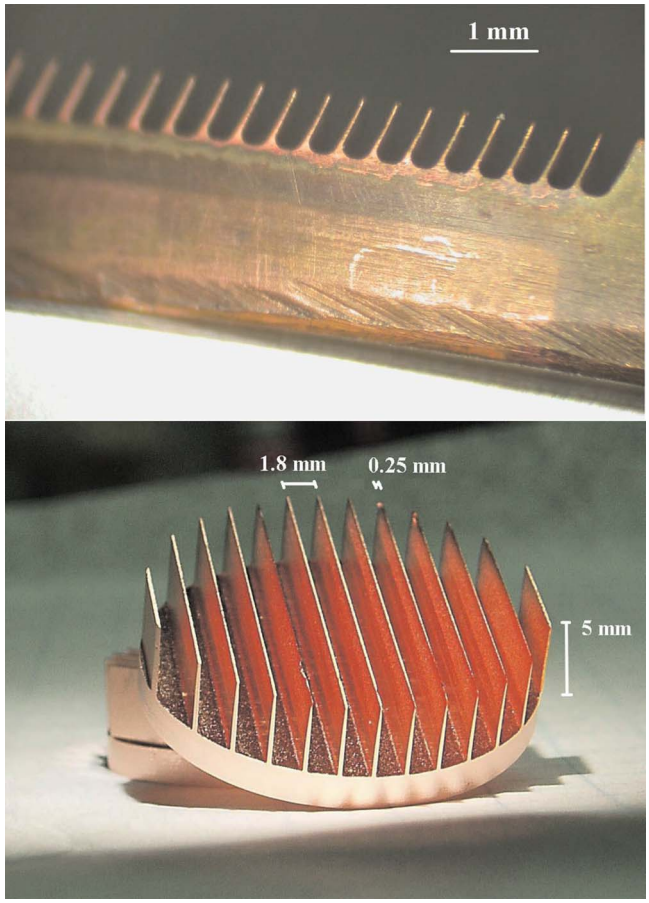

FIG. 13. (Color online) Grooved Cu samples. On the top figure the half flat and half slanted groove samples and on the bottom figure a fully rectangular Cu sample [$h \times a \times t = 5 \times 1.8 \times 0.254$ (mm)].

[This article is copyrighted as indicated in the article. Reuse of AIP content is subject to the terms at: http://scitation.aip.org/termsconditions. Downloaded to] IP: 35.8.11.3 On: Mon, 25 Jan 2016 00:27:02

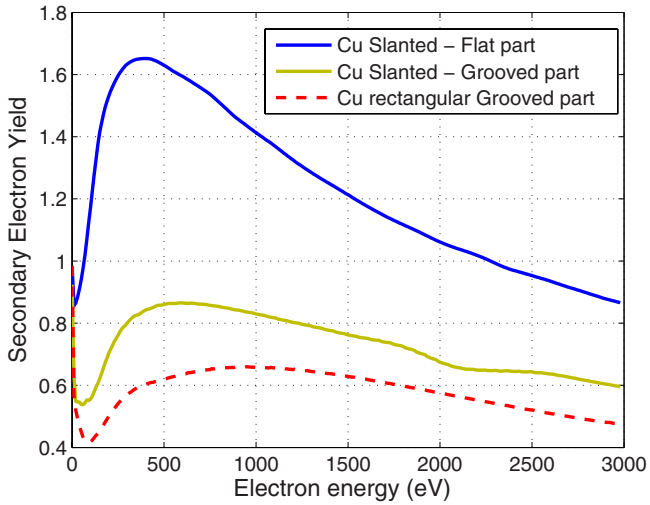

FIG. 14. (Color online) SEY reduction in the half slanted sample groove side compare to its flat part (solid line), see sample in Fig. 13 top figure. SEY reduction due to rectangular grooves of the sample shown in Fig. 13 bottom figure (dashed line).

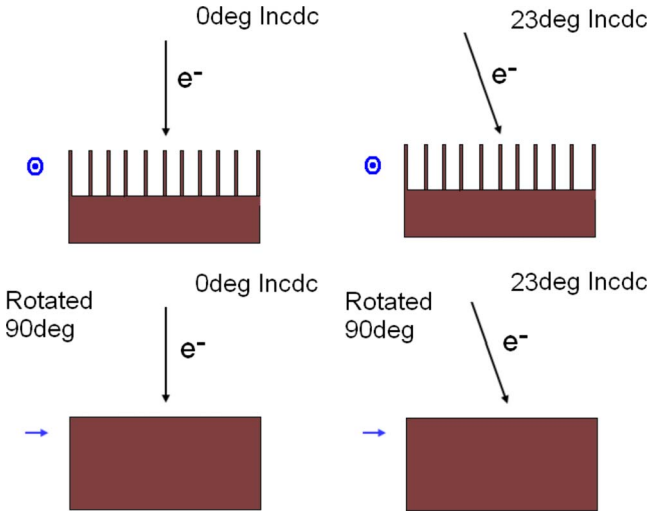

FIG. 16. (Color online) Layout of the experimental setup during the measurements of Fig. 15. The incidence angle of the electron beam and the sample rotation are shown. The blue arrows indicate the longitudinal direction of the rectangular grooves.

impinging electron beam relative to the surface normal. Results are shown in Fig. 15. The sample is first oriented as shown on the top part of Fig. 16, the electron beam rastering (scanning) from front to back. In this configuration, the impinging electron beam scans the inside of a valley (what is define by the letter "*a*" in Fig. 1) then a ridge (what is define by the letter "*t*" in Fig. 1), then the adjacent valley, and so on. Results are plotted in dashed lines in Fig. 15. When rotated 90°, the electron beam, still rastering from front to back, scans a point inside of a valley then a point on a ridge, then a point in the adjacent valley, and so on. Results are plotted in solid lines in Fig. 15.

Similarly to a flat surface, the more grazing the beam is, the higher the SEY, dashed lines comparison, Fig. 15. Since the primary electron beam did not scan the full sample, the sample was rotated 90° about its surface normal [see Fig. 16 bottom part and remeasured (solid lines)]. The results are

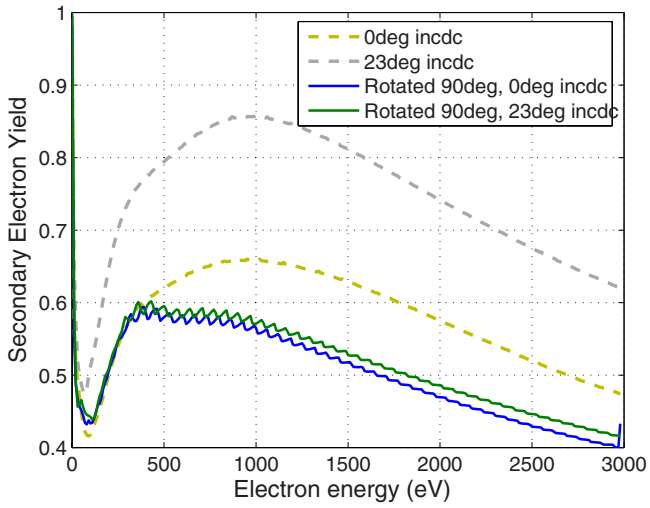

FIG. 15. (Color online) Variation in the SEY on the rectangular grooved Cu sample (Fig. 13 bottom figure) at 0° and 23° electron beam incidence angle respect to the normal of the surface and in function of the grooves orientation relative to the incoming electron beam.

similar to the results obtained when the electron beam is focused on one point down in the valley, no rastering mode. If the beam is focused on one point on top of a ridge the value of the SEY would be similar to the results obtained on a flat surface. Finally, as the energy of the electron beam increased, the scanned area becomes smaller. This is due to the designed construction of the electron gun.

Since the results obtained with Cu samples were very encouraging, we manufactured rectangular-grooved aluminum samples and then coat them with thin film TiN and TiZrV (NEG) coating, Fig. 17. Typically, the SEY maximum from a cleaned as received technical copper sample is between 1.6 to 2.2, while the peak SEY of as received technical aluminum is above 2.5.

Results for the TiN/Al and TiZrV/Al rectangular grooved samples are presented in Fig. 18 and Fig. 19. The SEY max is reduced below 1, as it was the case for the copper samples. In the case of the non-activated NEG sample $h/a=5$, $h/b=2.5$, and $a/t=1$, the value of the SEY measured and shown in Fig. 19 fits well with the simulation prediction for the given parameters by Fig. 7. Furthermore, in the case of the NEG coated sample, the activation process reduces further the SEY. Upon activation TiZrV NEG, deposited on a flat surface, shows a reduction of the peak SEY from ~1.8 to around 1.2.[8]

Furthermore, it is interesting to note that there is generally a shift to higher values of the electron energy at which the peak SEY occurs, 500–1000 eV, for the cases of grooved surfaces, as shown in Figs. 11, 12, 14, 15, 20, and 21. It is plausible that in the case of grooves, electrons are incident at smaller grazing angles; primary electrons make more secondary electrons near the surface, until finally the beam penetrates too deeply. We believe the shift in energy does not come from rastering or the sample direction of orientation during measurements. Nevertheless, the pattern is not always toward higher energies; for example, at least in one case, namely the TiN coated sample of Fig. 11, the shift is toward lower energies.

[This article is copyrighted as indicated in the article. Reuse of AIP content is subject to the terms at: http://scitation.aip.org/termsconditions. Downloaded to] IP: 35.8.11.3 On: Mon, 25 Jan 2016 00:27:02

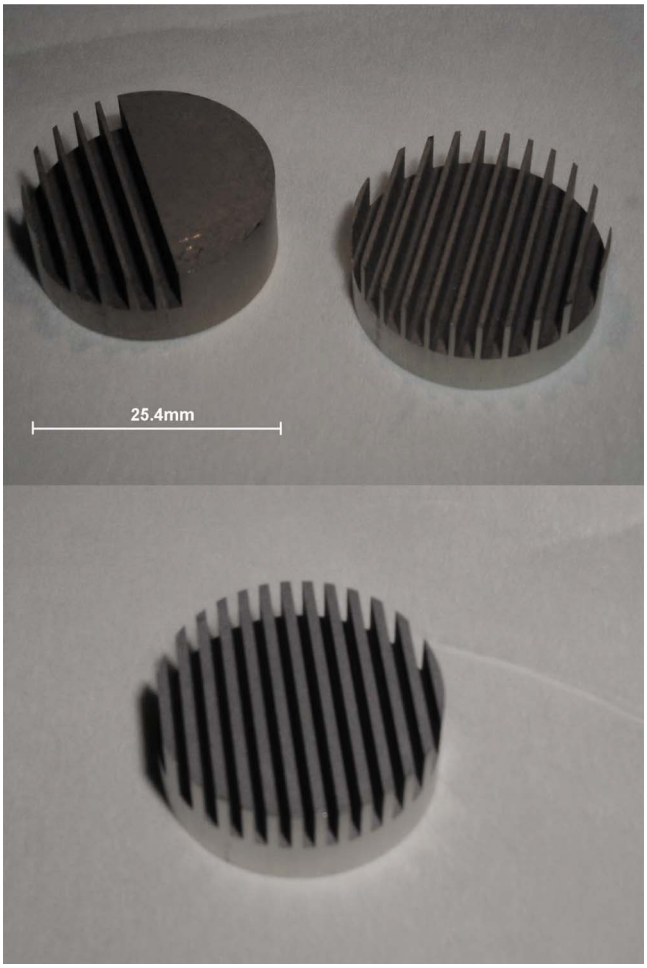

FIG. 17. (Color online) TiN/Al sample ($h \times a \times t = 5 \times 1.88 \times 0.6$ [mm]) top picture and TiZrV/Al ($h \times a \times t = 5 \times 1 \times 1$ [mm]) bottom picture. Samples were coated at the Lawrence Berkeley National Laboratory.

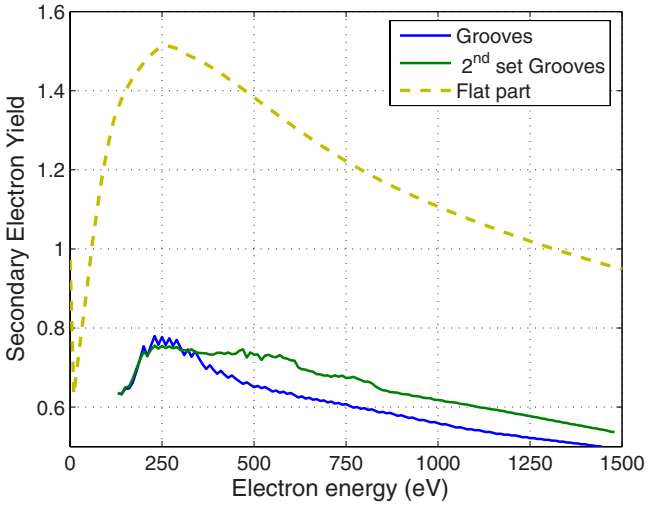

FIG. 18. (Color online) SEY reduction in a grooved TiN coated Al sample, see sample in Fig. 17 top figure. Comparison between the rectangular grooves, rastered, and the flat part.

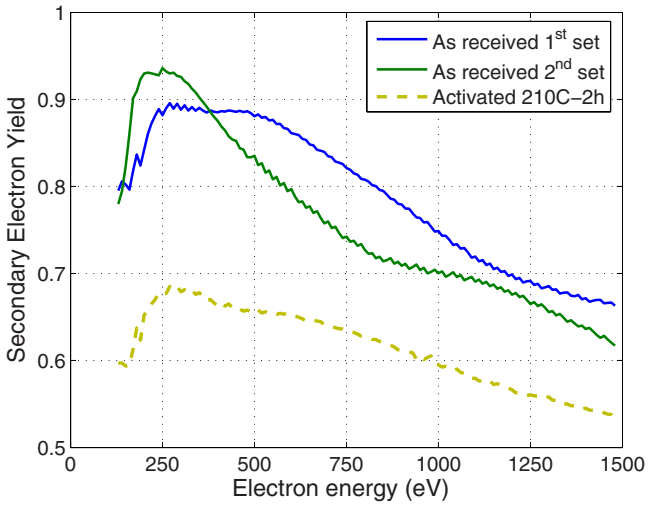

FIG. 19. (Color online) SEY reduction in a grooved TiZrV getter coated Al sample, see sample Fig. 17 bottom figure. SEY comparison between nonactivated and activated NEG.

V. COMPARISON BETWEEN SIMULATIONS PREDICTIONS AND EXPERIMENTAL RESULTS

In this section, we present a comparison summary of simulations and experimental observation for the groove samples shown in the paper. Simulations typically proceed in two steps: in a first simulation run the input parameters are chosen to fit the SEY curve of the sample surface flat side, which is then used as a reference. Once the parameters for the flat surface are obtained, a second simulation run is launched for a groove surface profile and results are compared to observations. For the purpose of the following discussion, let us define the electron reflectivity as the value of the SEY at the limit of 0 eV incident electron energy.

We have run simulations for the copper and TiN/Al rectangular groove samples. Figure 20 shows experimental observation compared to simulations for the copper rectangular groove sample shown in Figs. 13–15. The initial SEY is reduced by 60% and it is well below unity. Simulations indicate a reduction in the SEY very close to the experimental

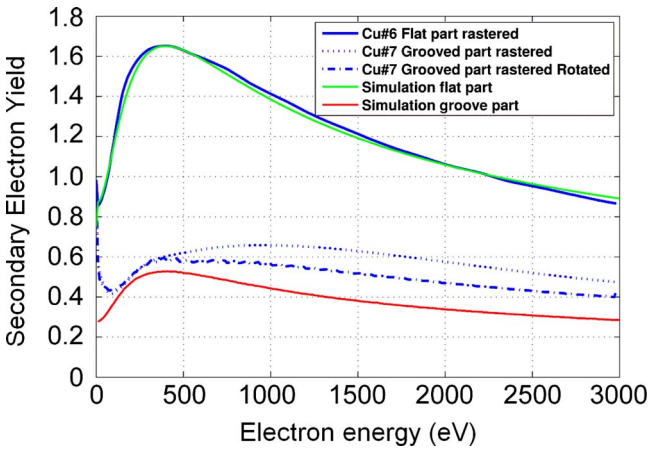

FIG. 20. (Color online) Experimental observation compared to simulations. The figure shows the results for the Cu rectangular groove sample shown earlier in Figs. 13–15.

[This article is copyrighted as indicated in the article. Reuse of AIP content is subject to the terms at: http://scitation.aip.org/termsconditions. Downloaded to] IP: 35.8.11.3 On: Mon, 25 Jan 2016 00:27:02

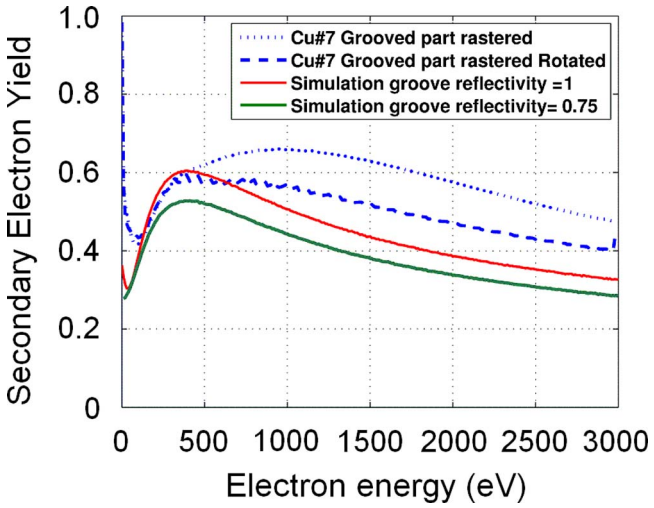

FIG. 21. (Color online) Comparison between two different simulations for the copper sample of previous Fig. 20, when assuming different SEY values (electron reflectivity) at 0 eV electron energy. The cases of reflectivities =0.75 and 1.0 are shown.

observation within ~15%. In the following Fig. 21, we show a comparison of two simulation results for the same sample, when assuming different electron reflectivities. The agreement is closer to the observation when assuming a reflectivity of 1.0, discussed in Ref. 21. Figure 22 shows a comparison of experimental observations and simulations for the TiN/Al rectangular groove sample shown in Figs. 17 and 18. Simulations indicate a reduction in the secondary electron in very good agreement to the experimental observation.

Furthermore, we have run simulations for the triangular groove sample of Fig. 11. An important consideration is that the simulation code does not yet include the roundness of the groove tips and valleys due to the manufacturing. The roundness is an important factor, which typically increases the SEY due to the reduction in effective inclined grooved surface. The profile of the triangular sample is shown Fig. 23. Simulations for the ideal triangular profile gave a 30% lower

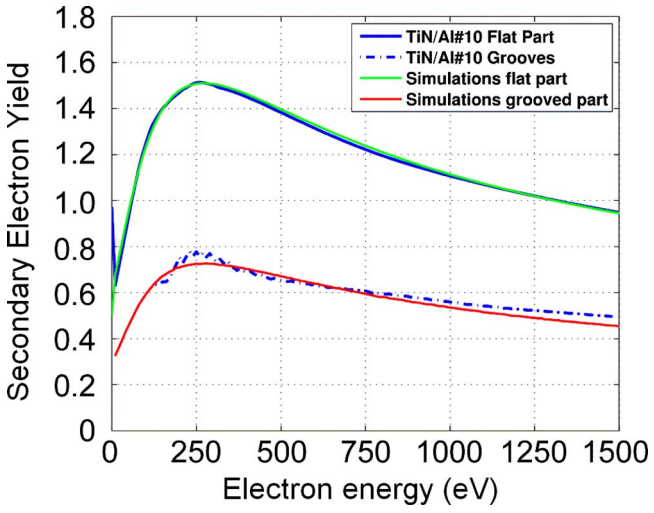

FIG. 22. (Color online) Experimental observation compared to simulations. The figure shows the comparison for the TiN/Al rectangular groove sample shown in Figs. 17 and 18.

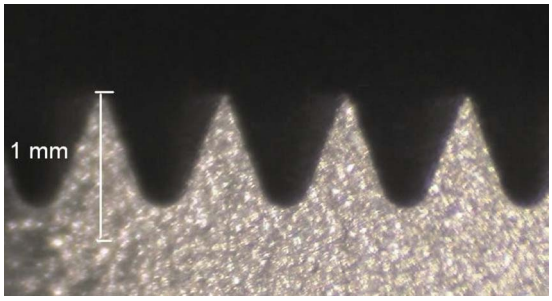

FIG. 23. (Color online) Close up of the aluminum triangular groove profile as previously shown in Fig. 11. In particular, note that the roundness of the valley is pronounced due to the particular manufacturing technique adopted. Roundness typically increases the SEY. The sample have been subsequently coated with TiN.

SEY with respect to the measured one. To properly compare simulations with experiments, the code would need to be upgraded to include the roundness. Nevertheless, the simulations of the triangular groove samples gave a good qualitative indication of the reduction in the SEY in the case of an ideal shape and offered insight to further improve the triangular groove design. In the case of rectangular grooves, the importance of roundness is much reduced due to both improved manufacturing techniques and deeper grooves.

VI. SUMMARY AND DISCUSSION

We presented results of computer simulations showing that one can suppress SEY using grooves on the surface of the vacuum chamber. The magnitude of suppression depends on the angle of triangular grooves and the aspect ratio of rectangular grooves. The measurements were performed in a magnetic field-free region. Simulation and experiments are in good agreement. Roundness results in an enhancement of the SEY.

Without magnetic field, the suppression depends only on dimensionless parameters that characterize the geometry of the grooves. In the case of triangular shapes, this parameter is the angle α. For rectangular grooves there are two such parameters: the aspect ratio h/a and the fraction a/t of the surface occupied by grooves. In case of magnetic field, in the limit $r_L \to 0$, the suppression in triangular grooves also depends only on the angle α. Triangular grooves are to be preferred in magnetic field region, since rectangular grooves are effective only when the separation between grooves is comparable to the electron's gyration radius $a \lesssim 2r_L$, which might be a technical challenge in the case of strong magnetic fields.

For the cases considered in this paper, we found that SEY suppressions in magnetic field require triangular grooves with small angles. We address the reader to the Refs. 15 and 16 for more studies on triangular grooves.

One could ask about the merit of the grooved surface in a field free region, and in that case what would be more efficient, a solenoid field or a groove? To decrease beam instabilities driven by an electron cloud, it is crucial to reduce the electron cloud density at the chamber center near the beam. Solenoids confine the cloud at the wall and are very effective at reducing the central cloud density. Further-

[This article is copyrighted as indicated in the article. Reuse of AIP content is subject to the terms at: http://scitation.aip.org/termsconditions. Downloaded to] IP: 35.8.11.3 On: Mon, 25 Jan 2016 00:27:02

more, the solenoid has negligible effect on the beam impedance when compared to the grooves. Solenoid may also introduce beam coupling that needs to be corrected. From a practical point of view, the grooves have the advantage that they are just part of the chamber design, while the solenoid field would require additional electricity costs, power supplies, maintenance, etc. It would be worth to envision adopting both mitigations to offer the maximal suppression efficiency.

Different samples with different grooves geometries have been measured. All samples did show an improvement when comparing to a flat surface. However, the machining or extrusion of chamber made with the best measured geometries might increase costs. Some of the first Al grooved samples made with very thin ridges and narrow canyon showed damages on the ridges, which have occurred during the machining. Application of thin coating, with lower SEY than the bare technical metal, on top of the grooves have helped further reducing the SEY. The homogeneity of the coating along the profile of the groove is not an easy task, since the top of the grooves tend to be coated more than the side walls and the base. The two combined methods (grooving and coating) can be a solution for a high-performance vacuum chamber.

Introduction of grooves on the surface will change the properties of interaction between the circulating beam and the wall. To minimize the resistive wall impedance, grooves should be oriented along the beam orbit. Another consequence is that the beam electric field will be concentrated on the groove edges with a small penetration of the electric field to the bottom of the grooves. Due to this shielding, secondary electrons emitted near the bottom of the groove will experience a suppressed beam electric field. However, the electric field of the beam could trigger field emission from those edges.[22] Nevertheless, field emission will occur for total electric field in excess of a few GV/m and it would be unlikely to occur in machines as PEP-II or the ILC DR.[23] Finally, image currents of the beam will run on the ridges of the grooves. Calculation of the temperature rise on the ridges must be effectuated to ensure that ridges will not deform or bend, reducing the effect of the grooves.

ACKNOWLEDGMENTS

The authors are thankful to S. Heifets, L. Wang, and M. Venturini for very useful discussions. We gratefully thank D. Lee and A. Wolski of LBNL for providing the samples. This work is supported by the U.S. DOE under Contract Nos. DE-AC03-76SF00515 and DE-AC03-76SF00098.

[1] R. A. Kishek, Y. Y. Lau, L. K. Ang, A. Valfells, and R. M. Gilgenbach, Phys. Plasmas **5**, 2120 (1998).
[2] E. W. Hoyt, W. P. Schulz, Report No. SLAC-TN-75–003, Stanford linear Accelerator Center (1975).
[3] E. L. Garwin, F. K. King, R. E. Kirby, and O. Aita, J. Appl. Phys. **61**, 1145 (1987).
[4] A. J. Hatch, Nucl. Instrum. Methods **41**, 261 (1966).
[5] J. W. Noé. Nucl. Instrum. Methods Phys. Res. A, **328**, 291 (1993).
[6] V. Baglin, J. Bojko, O. Gröbner, B. Henrist, N. Hilleret, C. Scheuerlein, and M. Taborelli, European Particle Accelerator Conference Proceedings, Vienna, Austria, 2000.
[7] L. Galán, I. Montero, E. Román, M. Alfonseca, J. De Lara, M. Garcia, P. Lozano, D. Wolk, and D. Raboso, Surface Treatment and Coating for the Reduction of Multipactor and Passive Inter-modulation (PIM) Efects in RF Components, in *Fourth International Workshop on Multipactor, Corona, and PIM in Space Hardware* (Noordwijk, The Netherlands, 2003).
[8] F. Le Pimpec, F. King, R. E. Kirby and M. Pivi, Nucl. Instrum. Methods Phys. Res. A, **564**, 44 (2006).
[9] N. Phinney, N. Toge, N. Walker *et al.*, International Linear Collider ILC Reference Design Report No. ILC-REPORT-2007–001 (2007).
[10] A. Wolski, J. Gao, S. Guiducci *et al.*, Report No. LBNL-59449, Lawrence Berkeley National Laboratory (2006).
[11] A. A. Krasnov, Vacuum **73**, 195 (2004).
[12] G. Stupakov and M. Pivi, Report No. SLAC-TN-04–045, LCC-0145, Stanford Linear Accelerator Center (2004).
[13] M. Furman and G. Lambertson. Note Report No. LBNL-41123, Lawrence Berkeley National Laboratory (1997).
[14] M. A. Furman and M. Pivi, Phys. Rev. ST Accel. Beams **5**, 124404 (2002).
[15] L. Wang, T. Raubenheimer, and G. Stupakov, European Particle Accelerator Conference Proceedings, Edinburgh, Scotland, 2006.
[16] M. Venturini, M. Furman, J.-L. Vay, and M. Pivi, Particle Accelerator Conference Proceedings, Albuquerque, New Mexico, 2007.
[17] C. L. Foerster, H. J. Halama, and G. Korn, J. Vac. Sci. Technol. A **10**, 2077 (1992).
[18] I. R. Collins, V. Baglin and O. Gröbner, European Particle Accelerator Conference Proceedings, Stockholm, 1998.
[19] N. Mahne, V. Baglin, I. R. Collins, A. Giglia, L. Pasquali, M. Pedio, S. Nannarone, and R. Cimino, Appl. Surf. Sci. **235**, 221 (2004).
[20] F. Le Pimpec, F. King, R. E. Kirby, and M. Pivi, J. Vac. Sci. Technol. A **23**, 1610 (2005).
[21] R. Cimino, I. R. Collins, M. A. Furman, M. Pivi, F. Ruggiero, G. Rumolo, and F. Zimmermann, Phys. Rev. Lett. **93**, 014801 (2004).
[22] B. B. Levchenko, On Field Emission in High Energy Colliders Initiated by a Relativistic Positively Charged Bunch of Particles, Technical Report, arXiv:physics/0608135v1, 2006.
[23] B. B. Levchenko, personal communication, May 2007.

[This article is copyrighted as indicated in the article. Reuse of AIP content is subject to the terms at: http://scitation.aip.org/termsconditions. Downloaded to] IP: 35.8.11.3 On: Mon, 25 Jan 2016 00:27:02